Letter

Supercurrent transport through 1e-periodic full-shell Coulomb islands

D. Razmadze,[1,*] R. Seoane Souto,[1,2,3,*] E. C. T. O'Farrell,[1] P. Krogstrup,[1] M. Leijnse,[1,2] C. M. Marcus,[1] and S. Vaitiekėnas[1]

[1]*Center for Quantum Devices, Niels Bohr Institute, University of Copenhagen, 2100 Copenhagen, Denmark*
[2]*Division of Solid State Physics and NanoLund, Lund University, 22100 Lund, Sweden*
[3]*Instituto de Ciencia de Materiales de Madrid (ICMM), Consejo Superior de Investigaciones Científicas (CSIC), Sor Juana Inés de la Cruz 3, 28049 Madrid, Spain*

(Received 19 August 2023; revised 15 December 2023; accepted 21 December 2023; published 19 January 2024)

We experimentally investigate supercurrent through Coulomb islands, where island and leads are fabricated from semiconducting nanowires with fully surrounding superconducting shells. Applying flux along the wire yields a series of destructive Little-Parks lobes with reentrant supercurrent. We find Coulomb blockade with 2e peak spacing in the zeroth lobe and 1e average spacing, with regions of significant even-odd modulation, in the first lobe. Evolution of Coulomb-peak amplitude through the first lobe is consistent with a theoretical model of supercurrent carried predominantly by zero-energy states in the leads and the island.

DOI: 10.1103/PhysRevB.109.L041302

The interplay between the superconducting gap, Δ, and charging energy, E_C, in mesoscopic superconductors gives rise to intriguing phenomena sensitive to single electron charging events [1]. Early transport studies revealed that the parity of a superconducting island depends sensitively on the ratio between Δ and E_C [2–4]. In particular, structures with $\Delta > E_C$ can only be charged in multiples of 2e. Suppressing Δ by temperature or magnetic field allows 1e charging. Thanks to their unique characteristics, superconducting islands are used as the basis of various modern quantum devices, including Cooper-pair transistors [5–7], charge qubits [8,9], and sensitive photon detectors [10,11].

Subgap states, emerging in superconducting hybrids, introduce an additional energy scale that characterizes the transport properties of the systems [12–16]. In semiconductor-superconductor islands, the subgap-state energy, ε, can be tuned via gate voltage or spin-splitting fields, allowing for precise control of island parity [17–19]. Islands with states at $\varepsilon < E_C$ can host an odd number of electrons resulting in even-odd Coulomb blockade periodicity [20,21]; for $\varepsilon = 0$, the Coulomb blockade becomes 1e periodic, which has been studied in the context of trivial [22,23] and topological [24–28] superconductivity. Previous experiments on devices with superconducting leads showed supercurrent in the Coulomb blockade regime [29,30] and 4π-periodic current-phase relation [31–33], theoretically attributed to the interplay between the Josephson coupling and low-energy subgap states [34–37].

Here, we use Coulomb-blockade transport to study the enhancement of 1e-periodic supercurrent in hybrid islands defined in semiconductor-superconductor full-shell nanowires. A representative device is shown in Fig. 1(a). Applying magnetic flux along the wire induces the destructive Little-Parks effect [38], resulting in a characteristic sequence of reentrant supercurrent lobes, as previously observed in cylindrical (or roughly cylindrical) samples with diameters below the superconducting coherence length [26,39–41]. In the zeroth lobe, transport displays 2e-periodic features in the Coulomb blockaded regime. In contrast, the Coulomb blockade is roughly 1e periodic throughout the first lobe, with small even-odd modulations, displaying an overall conductance background enhancement in the middle of the lobe. By comparing the experiment to a theoretical model, we find that the measurements are consistent with the presence of low-energy states in all three device segments.

The measured devices consist of hexagonal InAs nanowires with epitaxial *in situ* Al grown on all six facets, forming a continuous, fully surrounding superconducting shell [26,42–44]. Two ∼100 nm segments of the Al shell were selectively etched to form gateable Josephson junctions, controlled by gate voltages V_L and V_R; see Fig. 1(a). The charge offset of the island between the two junctions was tuned by the gate voltage V_G. The wire ends were contacted with Al leads, deposited in a separate lithography step. The evolution of the current-phase relation with axial flux through these wires was recently investigated through a combination of interferometry experiments [45] and theoretical analysis [46,47]. We report Coulomb spectroscopy results from four devices. In the main text, we focus on data from device 1, comprising a 700 nm island. Supporting data from the other three devices, including one with a 300 nm island, are presented in the Supplemental Material [48]. Transport measurements were carried out using standard ac lock-in techniques in a dilution refrigerator with a three-axis vector magnet and base temperature of 20 mK.

Differential resistance, dV/dI, as a function of current bias, I, and axial magnetic field, B, in the open regime ($V_L = V_R =$ 2 V) reveals a series of superconducting lobes; see Fig. 1(b). The switching current is maximal in the zeroth lobe, reaching roughly 50 nA at $B = 0$. The supercurrent vanishes around $|B| \sim 55$ mT, corresponding to half flux quantum through the

[*]These authors contributed equally to this work.

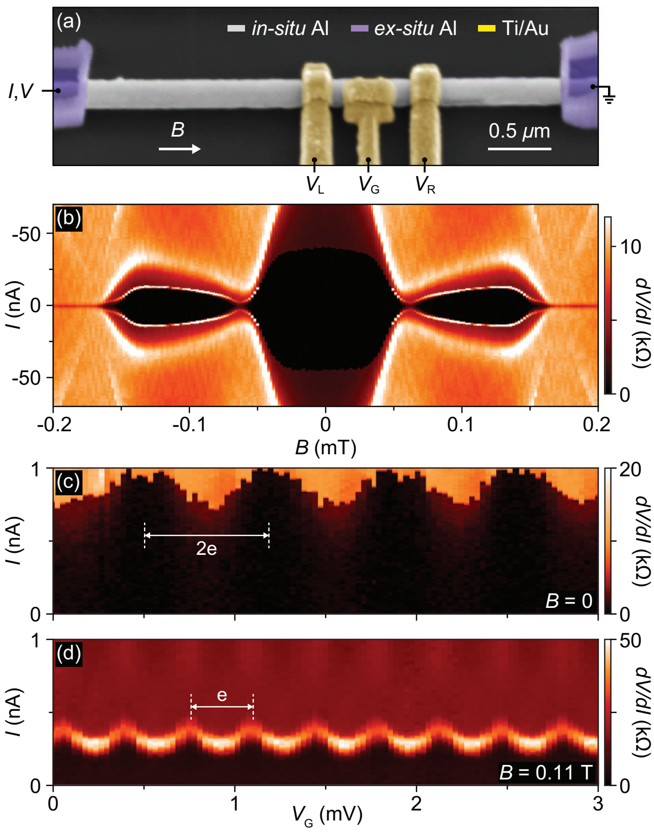

FIG. 1. (a) Color-enhanced electron micrograph of device 1 comprising hybrid InAs-Al full-shell Coulomb island. (b) Differential resistance, dV/dI, as a function of current bias, I, and axial magnetic field, B, displaying periodic Little-Parks modulation of the switching current as the magnetic flux threads the wire. The data were taken in the open regime ($V_L = V_R = 2$ V). (c) Zero-field dV/dI as a function of I measured in Coulomb blockade regime ($V_L = 55$ mV, $V_R = -182$ mV), showing $2e$-periodic switching current modulation as a function of island-gate voltage, V_G. (d) Same as (c) but measured at $B = 110$ mT, equivalent to one flux quantum threading the wire, showing roughly $1e$-periodic switching current modulation by V_G.

nanowire, but revives again at higher field values. In the first lobe, the maximal switching current of ∼15 nA is skewed toward the high-field end of the lobe. This is likely because the bound states carrying the supercurrent through the junctions have a smaller cross section compared to the parent Al shell and hence require a higher field to reach one flux quantum [43,49,50]. The two resistance steps in the zeroth and first lobes presumably result from different switching currents in two junctions. The sharp features, visible around $|B| \sim 170$ mT, can be associated with the switching current of the shell.

Lowering the junction-gate voltages decreases the Josephson coupling and increases the charging energy of the island, tuning the device into the Coulomb blockade regime. In this regime, the switching current oscillates as a function of V_G with a period of ∼0.7 mV around zero field [Fig. 1(c)] and roughly half of that at $B = 110$ mT [Fig. 1(d)]. The factor-of-two decrease in gate-voltage period suggests that Δ in the zeroth lobe exceeds E_C of the island, allowing for $2e$ charging. In the first lobe, $1e$ charging becomes possible due to

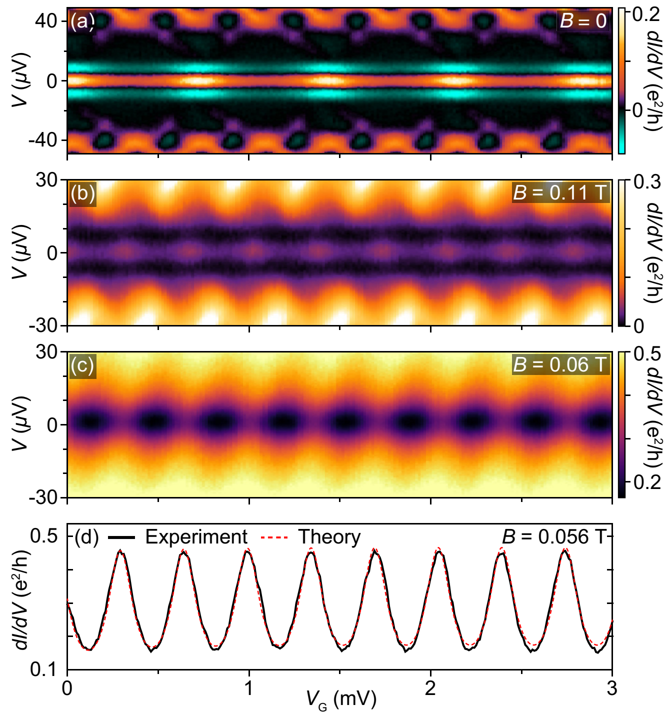

FIG. 2. Differential conductance, dI/dV, as a function of source-drain voltage bias, V, and island-gate voltage, V_G, in Coulomb-blockade regime ($V_L = -0.17$ V and $V_R = -0.3$ V), measured in (a) the zeroth lobe at $B = 0$, (b) the first lobe at $B = 110$ mT, and (c) the destructive regime at $B = 60$ mT. (d) Zero-bias conductance measured in the destructive regime at $V_L = -0.145$ V and $V_R = -0.45$ V (black curve), compared to a theoretical model (red-dashed curve) giving effective temperature of $T \sim 80$ mK and tunnel coupling to the two leads of $\hbar\Gamma_L \sim \hbar\Gamma_R/7 \sim 10$ μeV; see Ref. [48].

decreased spectral gap. The evenly spaced switching-current features at one flux quantum indicate the presence of subgap states, either continuous or discrete, near zero energy in the island.

To investigate the subgap excitations, we turn to Coulomb spectroscopy in a voltage-bias configuration. Differential conductance, dI/dV, as a function of voltage bias, V, and V_G, measured at $B = 0$ in the Coulomb blockade regime exhibits an extended supercurrent peak around $V = 0$; see Fig. 2(a). Peak height is modulated periodically by V_G but remains nonzero throughout the measured range. Additional features with half the period in V_G at higher bias correspond to multiple Andreev reflections that excite the island [51,52]. The first lobe displays a supercurrent peak similar to that of the zeroth lobe but with a halved period for its height modulations [Fig. 2(b)], consistent with the current-bias measurements in Fig. 1.

In the destructive regime between lobes, where superconductivity is suppressed, the device behaves as a metallic island coupled to normal leads. Transport through the system exhibits Coulomb diamonds without discrete features that extend continuously to zero bias, unlike in the superconducting lobes; see Fig. 2(c). Transport in this regime is well understood and can be used to extract effective electron temperature, T, and tunnel rates between the island and the

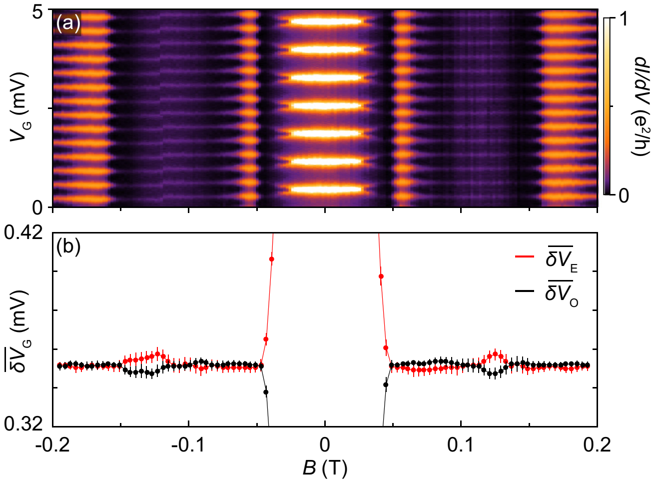

FIG. 3. (a) Zero-bias conductance, dI/dV, measured in the weak coupling regime ($V_L = -0.145$ V and $V_R = -0.45$ V), showing Coulomb blockade evolution as a function of island-gate voltage, V_G, and axial magnetic field, B. The Coulomb peaks display a locally enhanced conductance around one flux quantum ($|B| \sim 110$ mT). (b) Average peak spacing, $\overline{\delta V}$, for even (red) and odd (black) Coulomb valleys, extracted from the data in (a). Coulomb peaks are 2e periodic in the middle of the zeroth lobe, but split around $|B| = 40$ mT and become 1e periodic in the destructive regime ($|B| \sim 55$ mT). The peaks remain roughly 1e periodic with slight even-odd modulation throughout the first lobe.

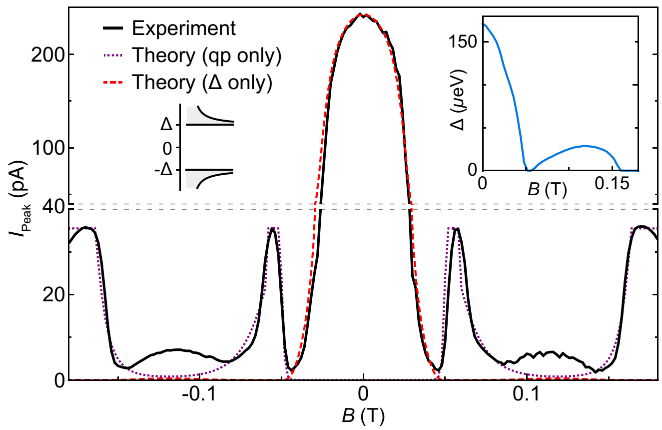

FIG. 4. Average Coulomb-peak current, I_{peak}, as a function of axial magnetic field, B. Experimental data (solid black curve) is extracted by integrating the differential conductance in Fig. 3(a) over the ac voltage excitation window. Normal quasiparticle current (dotted purple curve), calculated using Eq. (2), peaks in the destructive regimes and is exponentially suppressed in the superconducting lobes. Theoretical supercurrent (dashed red curve), calculated using the zero-bandwidth model with contributions only from the continuum states, shows a good agreement with the data in the zeroth lobe, but does not explain the bump in the middle of the first lobe. Inset: superconducting gap, Δ, as a function of B, used as an input for both theory curves, was extracted from an independent tunneling spectroscopy measurement; see Ref. [48].

leads, Γ_L and Γ_R [53]. Comparison of the zero-bias conductance to an expanded theory model [48] yields $T \sim 80$ mK and $\hbar\Gamma_L \sim \hbar\Gamma_R/7 \sim 10$ μeV.

Focusing on zero-bias features, we study the evolution of Coulomb-peak periodicity with B [Fig. 3(a)]. In the zeroth lobe, Coulomb peaks are 2e periodic up to $|B| \sim 40$ mT, then split as Δ decreases below E_C. A comparison with an independent gap measurement at the crossover point yields $E_C = 120$ μeV [48]. For larger B, the peaks continue splitting, becoming 1e periodic around $|B| = 55$ mT, at the onset of the destructive regime. At yet higher field, in the first lobe, the peaks remain nearly 1e periodic with slight even-odd modulation. We note that the conductance is finite for all gate-voltage values throughout the first lobe, consistent with the data in Fig. 2(b). Deviation from 1e periodicity is evident in the extracted average peak spacings, δV_G, for even and odd Coulomb valleys, shown in Fig. 3(b). The oscillatory behavior suggests a discrete subgap state crossing zero energy.

Further analysis of peak spacings yields the lowest excitation energy [54],

$$\varepsilon = E_C \, \frac{\overline{\delta V}_E - \overline{\delta V}_O}{\overline{\delta V}_E + \overline{\delta V}_O}, \qquad (1)$$

where $\overline{\delta V}_{E(O)}$ is the ensemble-averaged gate-voltage spacing of even (odd) Coulomb peaks. In the first lobe, the maximal even-odd peak spacing difference of $\sim$10 μV is consistent with a subgap state in the island with $\varepsilon = 2$ μeV. This value agrees with previously reported values for islands of similar length [26]. We note that device 4, with a shorter (300 nm) island, shows a larger even-odd peak spacing difference. When expressed in energy units, the difference corresponds roughly to the superconducting gap in the first lobe [48].

In addition to the even-odd peak spacing modulation in the first lobe, we observe a nonmonotonic peak height dependence, displaying a maximum in the middle of the lobe; see Fig. 3(a). This behavior is qualitatively consistent across different configurations of junction-gate voltages and for the other two devices with 700 nm islands, but absent in shorter 300 nm islands [48] and devices with normal leads [26]. To better understand this feature, we develop a model of supercurrent flow through the island, considering electron pairing and charging energy on equal footing (see the Supplemental Material [48]). The continuum states and the subgap states in the first lobe are described using the zero-bandwidth approximation [55–57].

To compare the model to experiment, we integrate the average Coulomb-peak conductance over the ac voltage excitation amplitude (2 μV) to obtain the measured current, I_{peak} (solid black curve in Fig. 4). We estimate the normal quasiparticle current using

$$I_{\mathrm{qp}} = I_N \exp\left[-\Delta(B)/k_B T\right], \qquad (2)$$

with independently measured electron temperature [Fig. 2(d)], field-dependent gap, $\Delta(B)$, (Fig. 4, inset), and the normal-state current, I_N, taken from the destructive regime (dotted purple curve in Fig. 4). Note that, away from the destructive regime, I_{qp} is suppressed exponentially and the experimental I_{peak} can be taken as a proxy of supercurrent flowing through the island.

The supercurrent from the states in the continuum was calculated by fitting the tunnel amplitude and using

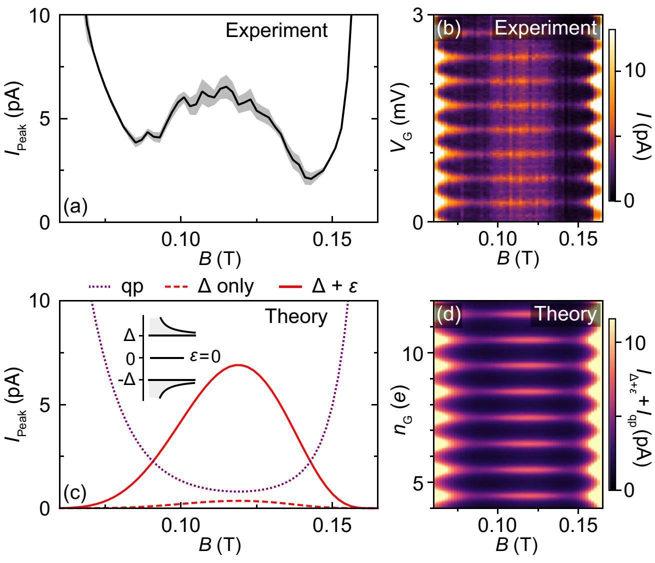

FIG. 5. (a) Average Coulomb-peak current, I_{peak}, from the data in Fig. 3(a), as a function of axial magnetic field, B. The gray band indicates the uncertainty from standard deviation of the peak heights. (b) First-lobe current, I, generated in response to the ac voltage excitation, as a function of island-gate voltage, V_G, and B. (c) Theoretical current through the device as a function of B. Dotted purple curve is the quasiparticle current given by Eq. (2). Dashed red curve is the calculated supercurrent contribution only from the states in the continuum. Solid curve is the calculated supercurrent, including the contribution from zero-energy subgap states in both leads and the island. (d) Calculated current in the first lobe as a function of charge offset, n_G, and B, including the normal quasiparticles' current and the supercurrent contributions from the continuum and zero-energy subgap state.

independently obtained values for effective temperature and tunnel-rate ratio [Fig. 2(d)], $\Delta(B)$, and zero-field I_{peak} (see the Supplemental Material [48] and Refs. [58,59] therein for details). Absent the inclusion of subgap states, the model agrees with the experiment in the zeroth lobe but fails to capture the observed bump in I_{peak} in the middle of the first lobe (compare solid black and dashed red curves in Fig. 4).

We next examine the simplest extension of the model by including a single subgap state at $\varepsilon = 0$ in the two leads and the island. We account for the change in localization length by linearly scaling the bound-state coupling rates with Δ. The resulting supercurrent effectively reproduces the experimental data, providing an explanation for the current enhancement observed in the middle of the first lobe [Figs. 5(a) and 5(c)]. The combined supercurrent model and quasiparticle current variation with charge offset on the island qualitatively captures the gate dependence of the measured Coulomb blockade in the first lobe [Figs. 5(b) and 5(d)]. Within the model, the observed even-odd peak spacing [Fig. 3(b)] can be interpreted as resulting from a nonzero-energy subgap state in the island. The uniform Coulomb peak heights suggest that the subgap state consists of equal electron and hole components [19,60]. For $\varepsilon = 0$, the Cooper-pair splitting process that is typically virtual during supercurrent transport becomes real. Increasing ε in the leads does not affect the peak spacing; instead, it suppresses the supercurrent, suggesting that the supercurrent enhancement observed in the middle of the first lobe requires low-energy subgap states in all three wire segments [48]. We note that our phenomenological model is insensitive to the origin of the subgap states. Nevertheless, our findings are fully consistent with previous studies reported in Refs. [26,45].

In summary, we have studied the supercurrent transport through a Coulomb island embedded in semiconducting (InAs) nanowires with a superconducting (Al) full shell. Applying an axial magnetic field to the wire resulted in the destructive Little-Parks effect with a reentrant supercurrent around one flux quantum. In the weak coupling regime, the island displayed $2e$-periodic Coulomb blockade peaks close to zero field. Around one flux quantum, the peaks were roughly $1e$ periodic and showed a local enhancement in conductance proportional to the supercurrent through the system. To explain the observed behavior, we used a zero-bandwidth model and showed that the supercurrent enhancement can only be explained by including low-energy subgap states in both leads and the island. These states enable a supercurrent transport mechanism that includes Cooper-pairs splitting, allowing for resonant tunneling of single electrons.

We thank C. Sørensen for contributions to materials growth and S. Upadhyay for assistance with nanofabrication. We acknowledge support from research grants (Projects No. 43951 and No. 53097) from VILLUM FONDEN, the Danish National Research Foundation, the Spanish CM "Talento Program" (Project No. 2022-T1/IND-24070), European Research Council (Grants Agreement No. 716655 and No. 856526), and NanoLund.

[1] D. V. Averin and Y. V. Nazarov, Phys. Rev. Lett. **69**, 1993 (1992).
[2] M. T. Tuominen, J. M. Hergenrother, T. S. Tighe, and M. Tinkham, Phys. Rev. Lett. **69**, 1997 (1992).
[3] P. Lafarge, P. Joyez, D. Esteve, C. Urbina, and M. H. Devoret, Phys. Rev. Lett. **70**, 994 (1993).
[4] P. Lafarge, P. Joyez, D. Esteve, C. Urbina, and M. H. Devoret, Nature (London) **365**, 422 (1993).
[5] A. J. Ferguson, N. A. Court, F. E. Hudson, and R. G. Clark, Phys. Rev. Lett. **97**, 106603 (2006).
[6] J. P. Pekola, J. J. Vartiainen, M. Möttönen, O.-P. Saira, M. Meschke, and D. V. Averin, Nat. Phys. **4**, 120 (2008).
[7] D. J. van Woerkom, A. Geresdi, and L. P. Kouwenhoven, Nat. Phys. **11**, 547 (2015).
[8] Y. Nakamura, Y. A. Pashkin, and J. S. Tsai, Nature (London) **398**, 786 (1999).

[9] J. Koch, T. M. Yu, J. Gambetta, A. A. Houck, D. I. Schuster, J. Majer, A. Blais, M. H. Devoret, S. M. Girvin, and R. J. Schoelkopf, Phys. Rev. A **76**, 042319 (2007).

[10] E. T. Mannila, V. F. Maisi, and J. P. Pekola, Phys. Rev. Lett. **127**, 147001 (2021).

[11] J. Tanarom, T. Watanabe, Y. Mizugaki, and H. Shimada, Appl. Phys. Express **15**, 064001 (2022).

[12] J.-D. Pillet, C. H. L. Quay, P. Morfin, C. Bena, A. L. Yeyati, and P. Joyez, Nat. Phys. **6**, 965 (2010).

[13] W. Chang, V. E. Manucharyan, T. S. Jespersen, J. Nygård, and C. M. Marcus, Phys. Rev. Lett. **110**, 217005 (2013).

[14] E. J. H. Lee, X. Jiang, M. Houzet, R. Aguado, C. M. Lieber, and S. D. Franceschi, Nat. Nanotechnol. **9**, 79 (2014).

[15] C. Jünger, R. Delagrange, D. Chevallier, S. Lehmann, K. A. Dick, C. Thelander, J. Klinovaja, D. Loss, A. Baumgartner, and C. Schönenberger, Phys. Rev. Lett. **125**, 017701 (2020).

[16] E. Prada, P. San-Jose, M. W. A. de Moor, A. Geresdi, E. J. H. Lee, J. Klinovaja, D. Loss, J. Nygård, R. Aguado, and L. P. Kouwenhoven, Nat. Rev. Phys. **2**, 575 (2020).

[17] A. P. Higginbotham, S. M. Albrecht, G. Kiršanskas, W. Chang, F. Kuemmeth, P. Krogstrup, T. S. Jespersen, J. Nygård, K. Flensberg, and C. M. Marcus, Nat. Phys. **11**, 1017 (2015).

[18] J. van Veen, A. Proutski, T. Karzig, D. I. Pikulin, R. M. Lutchyn, J. Nygård, P. Krogstrup, A. Geresdi, L. P. Kouwenhoven, and J. D. Watson, Phys. Rev. B **98**, 174502 (2018).

[19] S. Vaitiekėnas, R. S. Souto, Y. Liu, P. Krogstrup, K. Flensberg, M. Leijnse, and C. M. Marcus, Phys. Rev. B **105**, L041304 (2022).

[20] S. M. Albrecht, E. B. Hansen, A. P. Higginbotham, F. Kuemmeth, T. S. Jespersen, J. Nygård, P. Krogstrup, J. Danon, K. Flensberg, and C. M. Marcus, Phys. Rev. Lett. **118**, 137701 (2017).

[21] J. Shen, S. Heedt, F. Borsoi, B. van Heck, S. Gazibegovic, R. L. M. Op het Veld, D. Car, J. A. Logan, M. Pendharkar, S. J. J. Ramakers, G. Wang, D. Xu, D. Bouman, A. Geresdi, C. J. Palmstrøm, E. P. A. M. Bakkers, and L. P. Kouwenhoven, Nat. Commun. **9**, 4801 (2018).

[22] M. Valentini, M. Borovkov, E. Prada, S. Martí-Sánchez, M. Botifoll, A. Hofmann, J. Arbiol, R. Aguado, P. San-Jose, and G. Katsaros, Nature (London) **612**, 442 (2022).

[23] J. C. E. Saldaña, L. Pavešič, A. Vekris, K. Grove-Rasmussen, J. Nygård, and R. Žitko, Phys. Rev. B **108**, 224507 (2023).

[24] B. van Heck, R. M. Lutchyn, and L. I. Glazman, Phys. Rev. B **93**, 235431 (2016).

[25] S. M. Albrecht, A. P. Higginbotham, M. Madsen, F. Kuemmeth, T. S. Jespersen, J. Nygård, P. Krogstrup, and C. M. Marcus, Nature (London) **531**, 206 (2016).

[26] S. Vaitiekėnas, G. W. Winkler, B. van Heck, T. Karzig, M.-T. Deng, K. Flensberg, L. I. Glazman, C. Nayak, P. Krogstrup, R. M. Lutchyn, and C. M. Marcus, Science **367**, eaav3392 (2020).

[27] J. Shen, G. W. Winkler, F. Borsoi, S. Heedt, V. Levajac, J.-Y. Wang, D. van Driel, D. Bouman, S. Gazibegovic, R. L. M. Op het Veld, D. Car, J. A. Logan, M. Pendharkar, C. J. Palmstrøm, E. P. A. M. Bakkers, L. P. Kouwenhoven, and B. van Heck, Phys. Rev. B **104**, 045422 (2021).

[28] R. S. Souto, M. M. Wauters, K. Flensberg, M. Leijnse, and M. Burrello, Phys. Rev. B **106**, 235425 (2022).

[29] E. C. T. O'Farrell, A. C. C. Drachmann, M. Hell, A. Fornieri, A. M. Whiticar, E. B. Hansen, S. Gronin, G. C. Gardner, C. Thomas, M. J. Manfra, K. Flensberg, C. M. Marcus, and F. Nichele, Phys. Rev. Lett. **121**, 256803 (2018).

[30] J.-Y. Wang, C. Schrade, V. Levajac, D. van Driel, K. Li, S. Gazibegovic, G. Badawy, R. L. M. Op het Veld, J. S. Lee, M. Pendharkar, C. P. Dempsey, C. J. Palmstrøm, E. P. A. M. Bakkers, L. Fu, L. P. Kouwenhoven, and J. Shen, Sci. Adv. **8**, eabm9896 (2022).

[31] E. Bocquillon, R. S. Deacon, J. Wiedenmann, P. Leubner, T. M. Klapwijk, C. Brüne, K. Ishibashi, H. Buhmann, and L. W. Molenkamp, Nat. Nanotechnol. **12**, 137 (2017).

[32] D. Laroche, D. Bouman, D. J. van Woerkom, A. Proutski, C. Murthy, D. I. Pikulin, C. Nayak, R. J. J. van Gulik, J. Nygård, P. Krogstrup, L. P. Kouwenhoven, and A. Geresdi, Nat. Commun. **10**, 245 (2019).

[33] M. C. Dartiailh, J. J. Cuozzo, B. H. Elfeky, W. Mayer, J. Yuan, K. S. Wickramasinghe, E. Rossi, and J. Shabani, Nat. Commun. **12**, 78 (2021).

[34] L. Jiang, D. Pekker, J. Alicea, G. Refael, Y. Oreg, and F. von Oppen, Phys. Rev. Lett. **107**, 236401 (2011).

[35] F. Domínguez, O. Kashuba, E. Bocquillon, J. Wiedenmann, R. S. Deacon, T. M. Klapwijk, G. Platero, L. W. Molenkamp, B. Trauzettel, and E. M. Hankiewicz, Phys. Rev. B **95**, 195430 (2017).

[36] A. Vuik, B. Nijholt, A. R. Akhmerov, and M. Wimmer, SciPost Phys. **7**, 061 (2019).

[37] R. S. Souto and M. Leijnse, SciPost Phys. **12**, 161 (2022).

[38] W. A. Little and R. D. Parks, Phys. Rev. Lett. **9**, 9 (1962).

[39] Y. Liu, Y. Zadorozhny, M. M. Rosario, B. Y. Rock, P. T. Carrigan, and H. Wang, Science **294**, 2332 (2001).

[40] I. Sternfeld, E. Levy, M. Eshkol, A. Tsukernik, M. Karpovski, H. Shtrikman, A. Kretinin, and A. Palevski, Phys. Rev. Lett. **107**, 037001 (2011).

[41] S. Vaitiekėnas, P. Krogstrup, and C. M. Marcus, Phys. Rev. B **101**, 060507(R) (2020).

[42] P. Krogstrup, N. L. B. Ziino, W. Chang, S. M. Albrecht, M. H. Madsen, E. Johnson, J. Nygård, C. M. Marcus, and T. S. Jespersen, Nat. Mater. **14**, 400 (2015).

[43] A. Kringhøj, G. W. Winkler, T. W. Larsen, D. Sabonis, O. Erlandsson, P. Krogstrup, B. van Heck, K. D. Petersson, and C. M. Marcus, Phys. Rev. Lett. **126**, 047701 (2021).

[44] A. Ibabe, M. Gómez, G. O. Steffensen, T. Kanne, J. Nygård, A. L. Yeyati, and E. J. H. Lee, Nat. Commun. **14**, 2873 (2023).

[45] D. Razmadze, E. C. T. O'Farrell, P. Krogstrup, and C. M. Marcus, Phys. Rev. Lett. **125**, 116803 (2020).

[46] J. Schulenborg and K. Flensberg, Phys. Rev. B **101**, 014512 (2020).

[47] A. E. Svetogorov, D. Loss, and J. Klinovaja, Phys. Rev. B **107**, 134505 (2023).

[48] See Supplemental Material at http://link.aps.org/supplemental/10.1103/PhysRevB.109.L041302 for sample preparation and measurement details, additional data, and theoretical model description.

[49] A. A. Kopasov and A. S. Mel'nikov, Phys. Rev. B **101**, 054515 (2020).

[50] P. San-Jose, C. Payá, C. M. Marcus, S. Vaitiekėnas, and E. Prada, Phys. Rev. B **107**, 155423 (2023).
[51] A. M. van den Brink, A. A. Odintsov, P. A. Bobbert, and G. Schön, Z. Phys. B: Condens. Matter **85**, 459 (1991).
[52] P. Hadley, E. Delvigne, E. H. Visscher, S. Lähteenmäki, and J. E. Mooij, Phys. Rev. B **58**, 15317 (1998).
[53] J. M. Thijssen and H. S. J. Van der Zant, Phys. Status Solidi B **245**, 1455 (2008).
[54] S. Vaitiekėnas, A. M. Whiticar, M.-T. Deng, F. Krizek, J. E. Sestoft, C. J. Palmstrøm, S. Marti-Sanchez, J. Arbiol, P. Krogstrup, L. Casparis, and C. M. Marcus, Phys. Rev. Lett. **121**, 147701 (2018).
[55] I. Affleck, J.-S. Caux, and A. M. Zagoskin, Phys. Rev. B **62**, 1433 (2000).
[56] E. Vecino, A. Martín-Rodero, and A. Levy Yeyati, Phys. Rev. B **68**, 035105 (2003).
[57] K. Grove-Rasmussen, G. Steffensen, A. Jellinggaard, M. H. Madsen, R. Žitko, J. Paaske, and J. Nygård, Nat. Commun. **9**, 2376 (2018).
[58] J. C. Cuevas, A. Martín-Rodero, and A. Levy Yeyati, Phys. Rev. B **54**, 7366 (1996).
[59] E. Scheer, P. Joyez, D. Esteve, C. Urbina, and M. H. Devoret, Phys. Rev. Lett. **78**, 3535 (1997).
[60] E. B. Hansen, J. Danon, and K. Flensberg, Phys. Rev. B **97**, 041411(R) (2018).